Quantum Receiver for Distinguishing Between Binary Coherent-State Signals with Partitioned-Interval Detection and Constant-Intensity Local Lasers

Victor A. Vilnrotter*

ABSTRACT. — A quantum receiver concept capable of approaching the fundamental quantum limit on bit error probability is described and evaluated. Conventional optical and abstract quantum mechanical descriptions are provided and the underlying principles derived in both domains, thus providing a bridge to optimum quantum measurements in terms of well-understood optical communications concepts. Receiver performance is evaluated for the case of binary phase-shift keyed modulation, and it is shown that significant gains can be achieved over near-optimum receivers reported previously in the literature. This new receiver concept can be implemented using practical measurements amenable to high-rate operation, hence it may enable future deep-space optical communications with performance approaching the highest possible fidelity allowed by the laws of quantum mechanics.

I. Introduction

Deep-space optical communication is a key component of the NASA roadmap, with the goal of returning greater data volumes from Mars and other solar system encounters in future missions. Conventional optical receivers currently under consideration for deep-space communications employ photon-counting or coherent detection to potentially extract information even from a single photon, on the average. However, quantum mechanics promises greater gains, but fails to specify how these theoretical gains can be achieved in practice. So far, only a few schemes have been devised that are capable of approaching the theoretical quantum limit on bit-error probability (known as the Helstrom bound) over interplanetary distances, where diffraction losses prohibit the use of exotic quantum resources such as entanglement and squeezed states, limiting the choice to coherent states such as those produced by conventional laser transmitters that maintain coherence even with significant diffractive loss. The Dolinar receiver [1] was the first structured receiver that theoretically achieved the Helstrom bound using physically realizable measurements

* Communications Architectures and Research Section.

The research described in this publication was carried out by the Jet Propulsion Laboratory, California Institute of Technology, under a contract with the National Aeronautics and Space Administration. © 2012 California Institute of Technology. U.S. Government sponsorship acknowledged.

together with real-time optical feedback; however, practical implementation at high data rates was found to be challenging due to the requirement for precise local laser intensity control [2,3]. A different approach was proposed by Sasaki and Hirota [4], which does not employ optical feedback but achieves the Helstrom bound via unitary transformations and photon-counting. However, a practical implementation of the Sasaki-Hirota receiver requires multiphoton nonlinear optical processing, which also leads to complex receiver structures. The novel receiver structure proposed here overcomes these practical impediments by approaching the Helstrom bound using well-known practical measurements that enable high-speed implementation, while attaining significantly better performance than photon-counting, coherent detection, or even near-optimum quantum receivers such as the "Kennedy receiver," which is exponentially optimum and potentially implementable at high data rates [1,2,3].

The receiver processing considered here is motivated by recent results in quantum mechanics, according to which optimal quantum measurements on a binary signal can be attained by first partitioning the signaling interval into disjoint segments, then performing optimal measurements on each segment [5]. It is well known that for the case of small signal energies, coherent optical detection approaches the quantum limit, but degrades rapidly from the optimum measurement at higher signal energies. This observation suggests that if the signaling interval were partitioned into two disjoint segments, the first of short duration containing just enough signal energy to enable a near-optimum "predetection" measurement, and another higher-energy segment enabling more accurate detection by utilizing the information in the previous result, significant improvements in receiver performance might be possible. The approach analyzed here also provides new insights into the partitioned-interval detection process, casting the predetection segment in the framework of a quantum-optimum measurement that can be well approximated in the small-energy domain by classical methods such as field displacement and photon-counting, and furthermore helps to explain the connection between measurements in the classical and quantum domains.

II. Quantum Description of Communications Signals

In the classical model of optical communications, information can be incorporated in a laser beam by modulating the amplitude, phase, or polarization of the optical field. In the quantum model, information can be similarly incorporated into coherent states represented by the ket $|\alpha\rangle$ and described in [6]. Coherent states can be expressed in terms of the complete set of orthonormal number eigenstates $|n\rangle$ as

$$|\alpha\rangle = e^{-\frac{1}{2}|\alpha|^2} \sum_{n=0}^{\infty} \frac{\alpha^n}{(n!)^{1/2}} |n\rangle \tag{1}$$

The probability of observing n photons is Poisson with density $p(n) = |\alpha|^{2n} e^{-|\alpha|^2}/n!$, where $|\alpha|^2$ is the average number of photons. Coherent states are not orthogonal, as can be seen by considering the overlap of two arbitrary coherent states, $|\alpha\rangle$ and $|\beta\rangle$. Orthogonality requires that the overlap vanish; however, for coherent states the squared magnitude of the overlap is

$$|\langle \alpha|\beta \rangle|^2 = \left| e^{-(|\alpha|^2+|\beta|^2/2} \sum_n \sum_m \frac{\alpha^n}{\sqrt{n!}} \frac{(\beta *)^m}{\sqrt{m!}} \langle n|m \rangle \right|^2 = \left| e^{-(|\alpha|^2+|\beta|^2/2} \sum_n \frac{(\alpha\beta *)^n}{n!} \right|^2 = e^{-|\alpha-\beta|^2} \quad (2)$$

by virtue of the orthogonality of the number states $|n\rangle$. Equation (2) demonstrates that there is always some overlap between coherent states, regardless of how great the average photon count in each state may be [6,7].

Coherent states can be built up from the ground state by applying a displacement operator $D(\beta)$, whose action on the ground state yields $D(\beta)|0\rangle = |\beta\rangle$, as described in [8]. Similarly, coherent states can be transformed into other coherent states by the action of the displacement operator as follows: $D(\beta)|\alpha\rangle = |\beta + \alpha\rangle$. A practical way to implement the displacement operation is by the use of a local laser and a beam splitter, as described in [9]. Displacement of a received coherent state can be realized in the classical model by adding a small fraction of a local laser field of the same frequency as the received field through a high-transmission beam splitter.

It is informative to consider the binary problem of "on-off keying," whereby no signal pulse represents the null hypothesis H_0, whereas a laser pulse represents the alternate hypothesis H_1. In the quantum mechanical formulation, the received binary signal is represented by one of two coherent states $|\psi_0\rangle = |0\rangle$ or $|\psi_1\rangle$ corresponding to hypotheses H_0 and H_1. The signal field is assumed to be in a pure coherent state $|\alpha\rangle$, where α is a complex number and $|\alpha|^2$ represents the average number of photons in the signal. Photon-counting detection applies detection operators $\prod_0 |0\rangle\langle 0|$ and $\prod_1 = 1 - \prod_0$ to the signals, and declares H_0 if the ground state is observed, otherwise declares H_1 [7].

In the state-space interpretation of photon-counting developed in [7], two signal states define a plane in Hilbert space. Application of the photon-counting projection operators to the signal states generates "measurement states" [1] that span the two-dimensional subspace defined by the signal states, designated as $|w_0\rangle$ and $|w_1\rangle$ in Figure 1. The squared magnitude of the projection of each signal state onto its associated measurement state

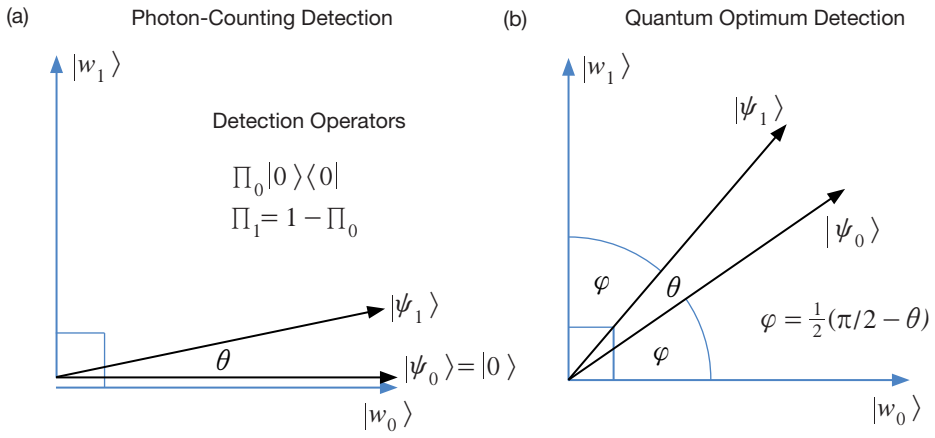

Figure 1. Measurement state interpretation of binary coherent state detection: (a) photon-counting; (b) optimum quantum measurement achieving the Helstrom bound.

is the probability that the signal state will be detected correctly. With this approach, the measurement state for H_0, $|w_0\rangle$ is taken to be the ground state, which corresponds to one of the two binary signals, as shown in Figure 1(a).

The measurement state for H_1, $|w_1\rangle$, does not in general align with any of the number states, but rather it is a superposition of number states except for the ground state, with coefficients determined by the signal state $|\psi_1\rangle$. A detailed description of this formulation is provided in [7].

The error probability is minimized and the Helstrom bound achieved when the two orthonormal measurement states are rotated symmetrically within the signal subspace, as shown in Figure 1(b). The resulting limit on the error probability has been derived in [7] by evaluating the signal-state projections onto each measurement state, and shown to be exactly equal to the Helstrom bound:

$$P^*(E) = \frac{1}{2}\left(1 - \sqrt{1 - 4p_0p_1|\langle\alpha|\beta\rangle|^2}\right) \tag{3}$$

In Equation (3), p_0 and p_1 are the a priori probabilities of H_0 and H_1, respectively. The measurement-state approach therefore provides a geometrical interpretation of the optimum quantum measurement, which allows us to relate the abstract quantum optimum measurement to classical measurements that can be carried out in a laboratory.

III. Near-Optimum Detection of BPSK Signals

Binary phase-shift keying (BPSK) modulation is particularly well suited to illustrating the key concepts in classical, near-optimum, and optimum quantum detection strategies, as well as establishing a correspondence between classical and quantum receiver performance. An example of BPSK signaling is shown in Figure 2: during each T-second symbol interval, the amplitude of the electric field is taken to be E if the binary data is "1," corresponding to hypothesis H_1, and $-E$ if the binary data is "0," corresponding to H_0. The signal amplitude therefore toggles between $\pm E$ in response to the data, but remains constant during each T-second symbol-interval. Assume that H_0 and H_1 occur with a priori probabilities p_0, p_1 respectively, where $p_0 + p_1 = 1$. The average photon count within each received symbol interval is $K_a = E^2T = |\alpha|^2$, while the actual photon count is k. The quantum representation of the binary signals is $|-\alpha\rangle$ when H_0 is true, and $|\alpha\rangle$ when the alternate hypothesis, H_1, occurs.

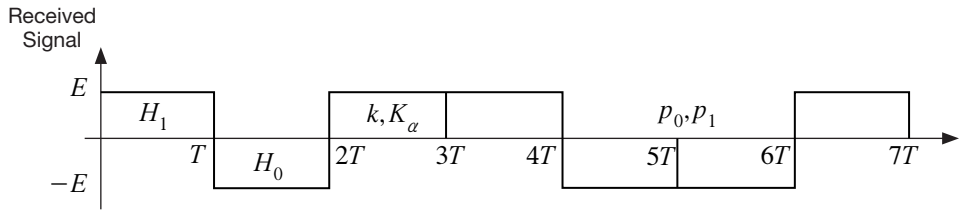

Figure 2. Classical representation of binary phase-shift keyed (BPSK) data stream.

A. Coherent Detection of BPSK Signals

Coherent detection of BPSK signals can be formulated as follows: the receiver adds a strong local laser field $|\beta| \gg |\alpha|$ to the signal with the same phase-angle, sets an optimum threshold η determined by solving the maximum a posteriori (MAP) decision rule for k, and decides by comparing the observed count to the threshold. With $p(k|H_i)$ denoting the probability of observing a count of k given hypothesis $H_i, i = 0, 1$, the MAP decision rule can be summarized as "select that hypothesis for which the weighted conditional density is greatest, given the observed photon-count k." Starting with the inequality $p_0 p(k|H_0) \gtrless p_1 p(k|H_1)$, then taking the natural log of both sides yields $\log_e(p_0/p_1) \gtrless k \log_e(|\beta + \alpha|^2/|\beta - \alpha|^2) - |\beta + \alpha|^2 + |\beta - \alpha|^2$: the optimum threshold η is that value that satisfies the inequality, namely

$$\eta = \frac{\log_e(p_0/p_1) + 4|\alpha||\beta|}{\log_e\left(|\beta + a|^2/|\beta - \alpha|^2\right)} \tag{4}$$

Based on the observed count, the coherent receiver declares H_1 if $k \geq \eta$, H_0 if $k < \eta$. Adding a local laser field can be viewed as an application of the displacement operator, yielding $D(\beta)|-\alpha\rangle = |\beta - \alpha\rangle$ and $D(\beta)|\alpha\rangle = |\beta + \alpha\rangle$, with energies $|\alpha - \beta|^2 = K_\alpha + K_\beta - 2\sqrt{K_\alpha K_\beta} \equiv K_{(-)}$ and $|\alpha + \beta|^2 = K_\alpha + K_\beta + 2\sqrt{K_\alpha K_\beta} \equiv K_{(+)}$, respectively. Note that the optimum threshold in Equation (4) is valid for any value of α and β, provided they have the same phase angle. The optimum threshold as a function of $|\alpha|^2$ is shown in Figure 3, for various values of displacement $|\beta|^2$ that minimized the error probability of the optimized Kennedy receiver, as will be described in a subsequent section. The key point to note is that in the range of $|\alpha|^2$ considered, namely $0 < |\alpha|^2 < 1$, the optimum threshold is always less than one, which means that the decision after photon-counting always depends on whether or not zero photons were observed. Note that whenever $|\alpha|^2 = |\beta|^2$, the optimum threshold actually becomes zero, since the denominator grows without bound at these points.

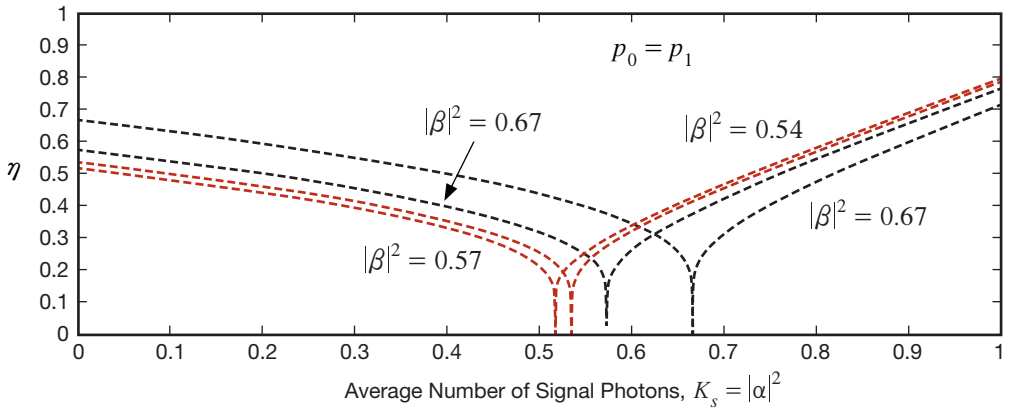

Figure 3. Optimum threshold for generalized coherent detection, as a function of $|\alpha|^2$ and $|\beta|^2$.

For the case of equal a priori probabilities $p_0 = p_1$ and $|\beta| \gg |\alpha|$, the limiting form of the error probability is given by the expression $P(E)_{|\beta| \gg |\alpha|} = \frac{1}{2}[1 - \mathrm{erf}(\sqrt{2K_\alpha})]$, where "erf " is the well-known error function defined as

$$\mathrm{erf}(x) = 2\pi^{-1/2} \int_0^x \exp(-t^2)\,dt$$

B. The Kennedy Receiver

A near-optimum detection strategy for binary signals was devised by R. S. Kennedy in 1974 [1]. The idea is to apply the displacement operator $D(\alpha)$ to the coherent states $|-\alpha\rangle, |\alpha\rangle$ before detection, yielding $D(\alpha)|-\alpha\rangle = |0\rangle$ and $D(\alpha)|\alpha\rangle = |2\alpha\rangle$. The displacement operator effectively converts the phase-modulated BPSK signals to on-off-keyed signals, but with twice the amplitude, hence four times the pulse energy, since now $|2\alpha|^2 = 4K_\alpha$. The displaced states are detected using photon-counting, yielding an average error probability $P(E) = \frac{1}{2}e^{-4K_\alpha}$, which is recognized as the error probability for equally probable on-off-keyed signals with average pulse energy $4K_\alpha$.

In terms of classical implementation, a constant phase-locked local laser field with amplitude E matched to the received field is first added to the signal using a beam-splitter, followed by conventional photon-counting detection. The negative BPSK symbols with amplitude $-E$ (corresponding to the null hypothesis H_0) are therefore converted to zero, whereas the positive symbols with amplitude E are converted to $2E$, as shown in Figure 4.

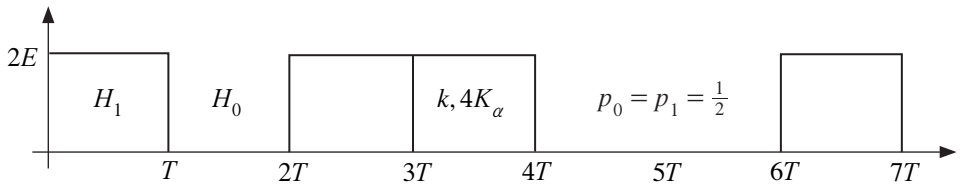

Figure 4. BPSK signals converted to on-off keyed signals via the Kennedy detection strategy.

The detection strategy is the same as for classical coherent detection, namely: set the optimum threshold defined in Equation (4) that is valid for all values of $|\beta|$, apply photon-counting detection, and declare H_1 if $k \geq \eta$, H_0 if $k < \eta$. However, note that for the case of equal a priori probabilities $\eta = 0$ since $\log_e(p_0/p_1) = 0$ and in addition as $|\beta| \to |\alpha|$ the optimum threshold approaches zero since the denominator grows without bound. Therefore, the detection strategy for the Kennedy receiver becomes: declare H_1 if $k > 0$, H_0 if $k = 0$. The relevant probabilities are given by

$$H_0\text{:}\quad p(k=0) = 1, \quad H_1\text{:}\quad \begin{cases} p(k=0) = \exp(-4K_\alpha) \\ p(k>0) = 1 - \exp(-4K_\alpha) \end{cases}$$

The conditional probabilities of correct detection become $P(C|H_0) = 1; P(C|H_1) = 1 - e^{-4K_a}$, which must be averaged over the a priori probabilities to obtain the average probability of correct detection: $P(C) = p_0 P(C|H_0) + p_1 P(C|H_1)$. Assuming equal a priori probabilities and substituting for the conditional probabilities yields the average probability of correct detection as $P(C) \underset{p_0 = p_1}{=} \frac{1}{2}(1 + [1 - \exp(-4K_\alpha)]) = 1 - \frac{1}{2}\exp(-4K_\alpha)$. The average error probability is related to the probability of correct detection as $P(E) = 1 - P(C)$; therefore, the average error probability of the Kennedy receiver is $P(E) \underset{p_0 = p_1}{=} \frac{1}{2}\exp(-4K_\alpha)$.

C. Limiting Behavior for Small Signal Energies

The error probabilities obtained above can be approximated for the case of vanishingly small signal energies, such that $4|\alpha|^2 \ll 1$. With conventional photon-counting, the conditional probabilities of correct detection for on-off keyed signals with amplitudes 0 and 2*E*, or equivalently represented by coherent states $|0\rangle, |2\alpha\rangle$, are $P(C|H_0) = 1$ and $P(C|H_1) = 1 - e^{-4|\alpha|^2} = 1 - 1 + 4|\alpha|^2 - \ldots \cong 4|\alpha|^2$. With equal a priori probabilities, $p_0 = p_1$, the average probability of correct detection can be approximated as

$$P(C) = \tfrac{1}{2}\{P(C|H_0) + P(C|H_1)\} \cong \tfrac{1}{2}(1 + 4|\alpha|^2)$$

which yields the average error probability $P(E) = 1 - P(C) \cong \frac{1}{2}(1 - 4|\alpha|^2)$ for Kennedy receiver detection of BPSK signals. Under the same conditions of small signal energy and equal a priori probabilities, $|\langle 0|2\alpha\rangle|^2 = e^{-4|\alpha|^2} \cong 1 - 4|\alpha|^2$, hence the Helstrom bound for the displaced states becomes

$$P^*(E) \cong \tfrac{1}{2}[1 - \sqrt{1 - (1 - 4|\alpha|^2)}] = \tfrac{1}{2}[1 - 2|\alpha|]$$

For small x, such that $x \ll 1$, the error function can be approximated by the first term in its Taylor's series expansion as $erf(x) \underset{x \ll 1}{\cong} 2\pi^{-1/2}x$, yielding the approximate error probability for coherent detection

$$P(E) \underset{\sqrt{2K_s} \ll 1}{\cong} \frac{1}{2}[1 - 2\sqrt{\tfrac{2}{\pi}}|\alpha|]$$

for the limiting case $|\beta| \gg |\alpha|$.

In order to compare the above small-energy error probabilities to the Helstrom bound for the original signals, compute the squared-overlap of the two signal states $|-\alpha\rangle, |\alpha\rangle$ corresponding to H_0, H_1, respectively, and substitute into Equation (3):

$$|\langle -\alpha|\alpha\rangle|^2 = \exp(-4|\alpha|^2) \underset{4|\alpha|^2 \ll 1}{\cong} 1 - 4|\alpha|^2$$

where the last approximation applies in the limit of small signal energies. Substituting into the Helstrom bound for the BPSK signal set, we again obtain

$$P^*(E) \underset{4|\alpha|^2 \ll 1}{\cong} \tfrac{1}{2}[1 - \sqrt{1 - (1 - 4|\alpha|^2)}] \underset{4|\alpha|^2 \ll 1}{\cong} \tfrac{1}{2}[1 - 2|\alpha|]$$

since a displacement of the signal states does not change their overlap. It can be inferred from Figure 5 that for signal energies less than approximately 0.02 photons, the simple approximations (dashed curves) are in good agreement with the exact results (solid curves), hence are useful in helping to understand and analyze limiting behavior. For example, with photon-counting detection, the error exponent is proportional to signal energy, yielding linear behavior with energy on a logarithmic plot. On the other hand, the coherent receiver is linear with field amplitude just as the Helstrom bound, hence behaves similarly, but since the coefficient of the linear term is smaller by a factor of $\sqrt{2/\pi}$ for the coherent receiver, it narrowly fails to reach the Helstrom bound even at small signal energies.

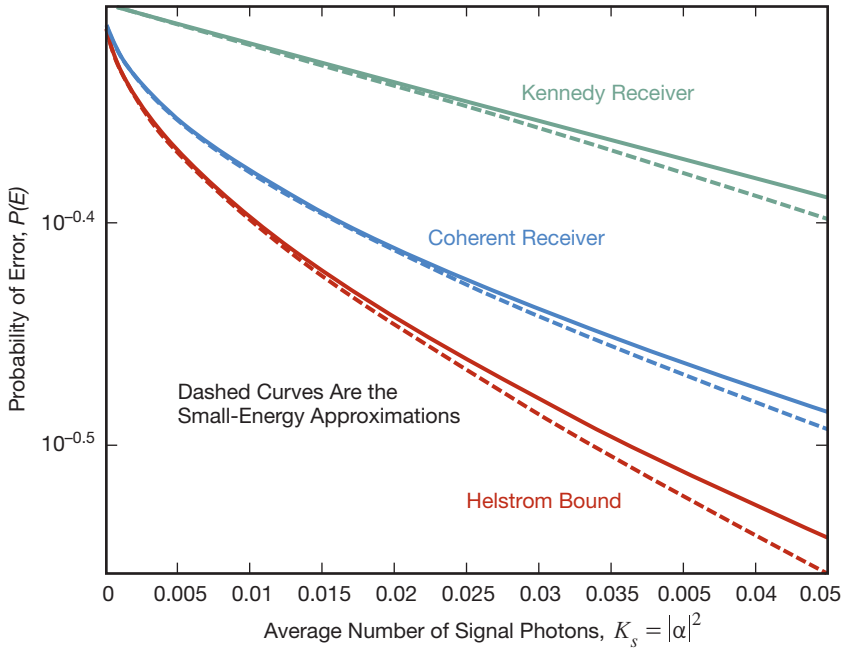

Figure 5. Exact error probabilities and small-energy approximations as functions of signal energy.

D. Approaching the Helstrom Bound via Signal-State Rotation

It is noteworthy that with the Kennedy receiver the cancelled signal always results in correct detection, since no photons can be observed in the absence of a signal pulse. In addition, doubling the signal amplitude for the alternate hypothesis increases the signal energy by a factor of four, greatly reducing the probability of a zero photon-count when a pulse is present: these are the primary reasons why the Kennedy receiver achieves near-optimum performance. However, photon-counting detection implies that one of the measurement states be aligned with the ground state, and as we have seen, this is not the condition under which optimum performance is achieved. The state-space representation of optimum detection described in [7] and illustrated in Figure 1(b) shows that the measurement states must be symmetrically arranged with the signal states for optimum detection, not asymmetrically as is the case with photon-counting detection. It is therefore natural to ask under what conditions optimum detection could be approached by starting with photon-counting detection, and rotating the signal-states into a more symmetrical configuration with respect to the measurement states.

An approximate state-space representation of photon-counting for small signal energies is shown in Figure 6(a), where the measurement states are approximated by the number states $|0\rangle$ and $|1\rangle$, so that $|w_0\rangle = |0\rangle$ and $|w_1\rangle = |1\rangle$. With photon-counting detection, the signal state representing H_0 is aligned with the measurement state, resulting in $|\psi_0\rangle = |w_0\rangle = |0\rangle$, whereas the alternate state $|\psi_1\rangle$ is rotated in the $|0\rangle, |1\rangle$ plane by an angle θ related to the overlap of the signal states as $\theta = \cos^{-1}(|\langle\psi_0|\psi_1\rangle|) = \cos^{-1}(e^{-\frac{1}{2}|2\alpha|^2})$: for example, with $|\alpha| = 0.2$, the angle between the signal states is $\theta = 22.6$ degrees.

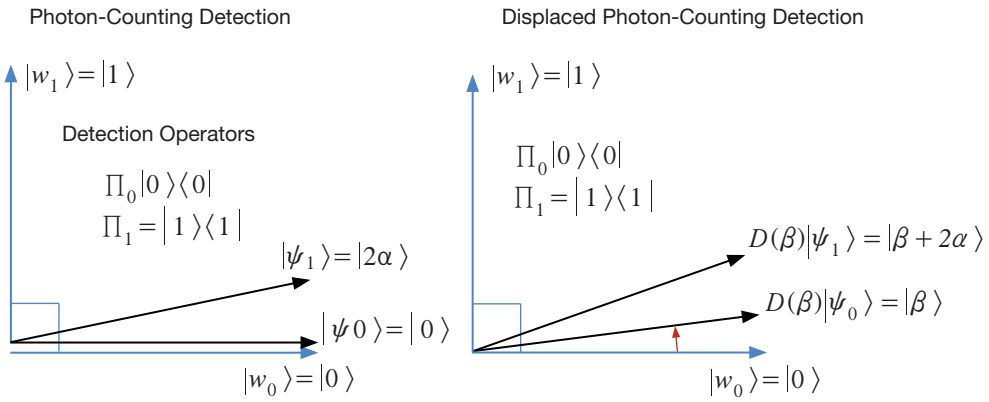

Figure 6. Small signal energy representation of photon-counting and displaced photon-counting.

Recall from Figure 1(b) that the measurement states are symmetrically placed around the signal states in the signal subspace, hence the optimum rotation angle is $\varphi = \frac{1}{2}(\pi/2 - \theta)$: for our example, the optimum rotation angle between the signal state $|\psi_0\rangle$ and its associated measurement state $|w_0\rangle$ should be $\varphi = 33.7$ degrees, the same as between $|\psi_1\rangle$ and $|w_1\rangle$. From the overlap relation for coherent states, an angle of 33.7 degrees corresponds to an overlap of $\cos(33.7) = 0.832 = e^{-\frac{1}{2}|\beta|^2}$, yielding a displacement magnitude of $|\beta| = 0.61$. The rotation could therefore be accomplished by applying the displacement operator $D(\beta)$ to the signal states as indicated in Figure 6(b), where $|\beta| = 0.61$ and $\arg(\beta) = \arg(\alpha)$. After displacement, the probability of finding $D(\beta)|\psi_0\rangle$ projected onto the next higher dimensional state $|2\rangle$, which begins to tilt the signal subspace from the two-dimensional $|0\rangle, |1\rangle$ subspace into the three-dimensional $|0\rangle, |1\rangle, |2\rangle$ subspace, is $p(k=2) = |\langle 2|\beta\rangle|^2 = |\beta|^4 e^{-|\beta|^2}/2 = 0.04$. This is acceptably small for justifying the two-dimensional measurement-state model; however, this probability increases to $|\langle 2|\beta + 2\alpha\rangle|^2 = 0.183$ for $D(\beta)|\psi_1\rangle$, which is significantly greater than zero and hence cannot be ignored. Similarly, the probability of finding $D(\beta)|\psi_0\rangle$ projected onto any of the higher-dimensional states $|2\rangle, |3\rangle, \cdots$ is equal to the probability that it is not projected onto the states $|0\rangle$ or $|1\rangle$: $p(k \geq 2) = 1 - \sum_{k=0}^{1} |\langle k|\beta\rangle|^2$. These probabilities are shown in Figure 7 as a function of $|\beta|$, increasing from 0 to 1.

With the help of Figure 7, we can argue that as long as the total displacement of the "pulse" state is less than approximately 0.2 to 0.3 in amplitude, the two-dimensional model should be accurate. For larger displacements, the projection onto third and higher dimensions starts to become significant, effectively tilting the signal subspace out of the two-dimensional $|0\rangle, |1\rangle$ subspace, hence the photon-counting interpretation is no longer accurate with larger displacements. This explains why displacement followed by photon-counting approaches the optimum quantum measurement for small signal energies, but fails to reach it completely. However, the small-energy model still provides theoretical insights into the manner in which displacement followed by photon-counting detection approximates the Helstrom bound for small signal energies, and suggests approaches that may result in better receiver performance when small signal energies are involved.

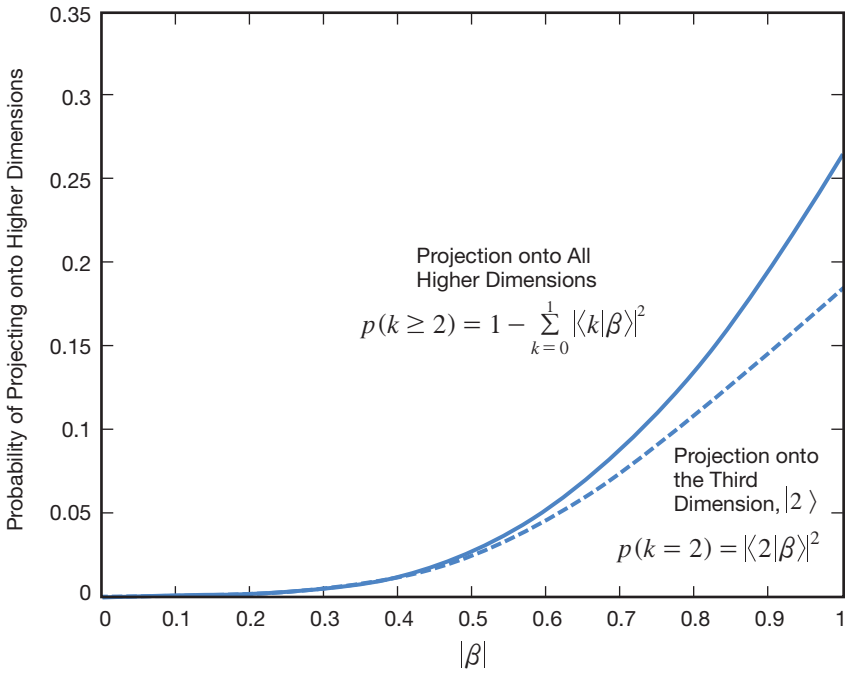

Figure 7. Probability of finding a displaced ground state projected onto higher number state dimensions.

E. The Optimized Kennedy Receiver

A displacement-optimized version of the Kennedy receiver, where the displacement does not cancel the null hypothesis exactly, but at the same time provides significant additional energy to the alternate, has been reported in [10,11], termed the "optimized displacement receiver." Since the displacement operator can be implemented with a strong local laser and a classical beamsplitter [9], the above discussion suggests that the performance of the Kennedy receiver could be improved in the small-signal-energy regime by first adding a phase-locked coherent field to the BPSK signals, detecting via photon-counting, then applying the optimum threshold defined in Equation (4), which is valid for all displacements. The classical signal model for BPSK signals after displacement is shown in Figure 8, where E_{LO} takes the place of the coherent state amplitude β.

The optimum value of the displacement for photon-counting detection can be derived by noting that for the small-energy region the value of the optimum threshold is always between 0 and 1. The goal of the optimization is to determine that value of β that maximizes the average probability of correct detection given β, $P(C) = \max_{\beta} P(C|\beta)$, or equivalently minimizes the average probability of error. With no loss in generality, assume that the signal amplitudes α, β are real, and write the conditional probabilities under the two hypotheses as $P(C|H_0,\beta) = \exp[-(\beta-\alpha)^2], P(C|H_1,\beta) = 1 - \exp[-(\beta+\alpha)^2]$. Differentiating the conditional probability of correct detection $P(C|\beta) = p_0 P(C|H_0,\beta) + p_1 P(C|H_1,\beta)$ with respect to β and solving, the following result is obtained:

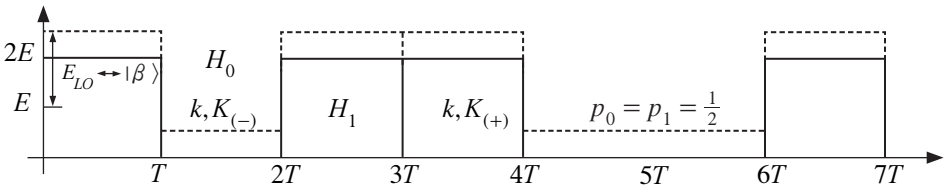

Figure 8. Classical model of displaced BPSK signals, for the optimized Kennedy receiver.

$$\frac{\partial}{\partial\beta}P(C|B) = 2p_0(\alpha-\beta)\exp[-(\beta-\alpha)^2] - 2p_1(\alpha+\beta)\exp[-(\beta+\alpha)^2] = 0 \tag{5a}$$

$$p_0(\beta-\alpha)\exp[-(\beta-\alpha)^2] = p_1(\beta+\alpha)\exp[-(\beta+\alpha)^2] \tag{5b}$$

$$\frac{p_0(\beta-\alpha)}{p_1(\beta-\alpha)} = \exp(-4\alpha\beta) \tag{5c}$$

The transcendental equation in Equation (5c) can be solved numerically, by evaluating the left and right sides of Equation (5c) as a function of β for each p_0, p_1 and α of interest, and finding that value of $\beta = \beta^*$ for which the two sides are equal. Letting the LHS be $f_1 \equiv p_0(\beta-\alpha)/p_1(\beta+\alpha)$ and the RHS be $f_2 = \exp(-4\alpha\beta)$, these are shown in Figure 9(a) as functions of $|\beta|^2$ for values of $|\alpha|^2 = 0.05, 0.1, 0.2, 0.4$, for the case of equal a priori probabilities.

The intersection of the two functions is indicated by small circles in Figure 9(a), and clearly show that as $|\alpha|^2 \to 0, |\beta^*|^2 \to 0.5$. The numerical values of the optimal displacement can be found very accurately by taking the magnitude of the difference of the two functions, $|f_1 - f_2|$, and finding the minimum, as shown in Figure 9(b).

The optimum values $|\beta^*|^2$ are also tabulated in Figure 11(b), for the four cases of $|\alpha|^2$ considered. This result is in contrast to the Kennedy receiver, where the signal fields are either

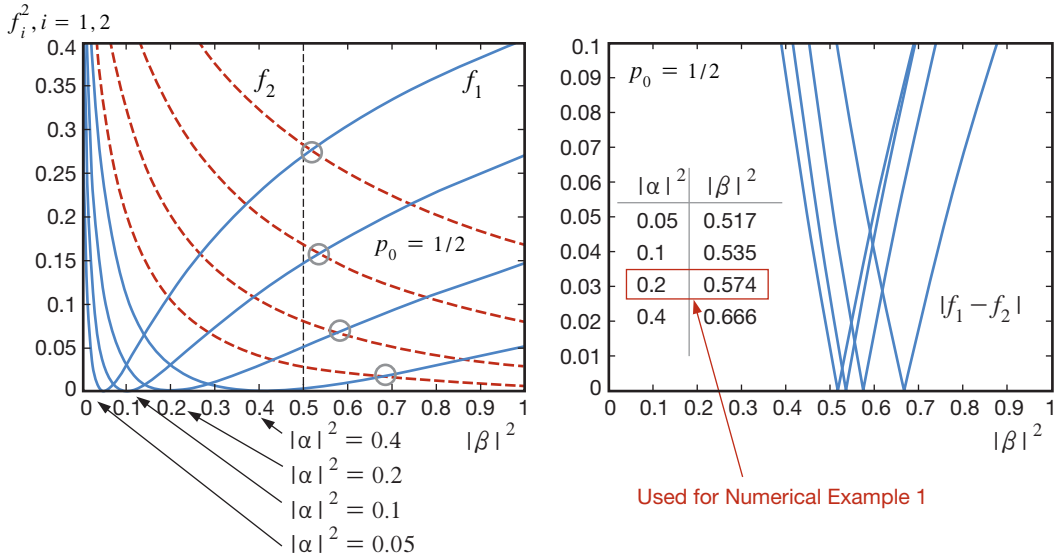

Figure 9. Numerical optimization of displacement for the optimized Kennedy receiver.

cancelled or reenforced by applying a displacement exactly equal to one of the BPSK signal amplitudes.

Applying the optimum displacement operator $D(\beta^*)$ to the binary signals results in the displaced signals $D(\beta^*)|-\alpha\rangle = |\beta^* - \alpha\rangle$ and $D(\beta^*)|\alpha\rangle = |\beta^* + \alpha\rangle$, with corresponding signal energies $|\beta^* - \alpha|^2 = K_\alpha + K_\beta - 2\sqrt{K_\alpha K_\beta} \equiv K_{(-)}$ and $|\beta^* + \alpha|^2 = K_\alpha + K_\beta + 2\sqrt{K_\alpha K_\beta} \equiv K_{(+)}$. After photon-counting detection over each symbol interval, the decision strategy calls for declaring H_1 if $k \geq \eta$, and H_0 if $k < \eta$. As before, η is the optimum threshold defined in Equation (4). Note that non-zero counts are now possible even under H_0 due to the optimal displacement, unlike with the Kennedy receiver, which displaced the signals suboptimally by completely cancelling one of them. The relevant probabilities for the general case are

$$H_0\colon\ \ p(k<\eta) = \sum_{k=0}^{\eta} K_{(-)}^k \exp(-K_{(-)})/k! \quad H_1\colon \begin{cases} p(k<\eta) = \sum_{k=0}^{\eta} K_{(+)}^k \exp(-K_{(+)})/k! \\ p(k<\eta) = 1 - \sum_{k=0}^{\eta} K_{(+)}^k \exp(-K_{(+)})/k! \end{cases}$$

For any signal energy, with optimal displacement the conditional probabilities of correct detection become $P(C|H_0) = p(k < \eta|K_{(-)})$; $P(C|H_1) = 1 - p(k < \eta|K_{(+)})$, which again has to be averaged over the a priori probabilities to obtain the average probability of correct detection, $P(C) = p_0 P(C|H_0) + p_1 P(C|H_1)$, finally yielding $P(E) = 1 - P(C)$. Due to the optimization of the displacement, these calculations are somewhat more involved than for the Kennedy receiver, as the following example illustrates.

Example 1. Consider the case where $|\alpha|^2 = 0.2, |\alpha| = 0.447$, $p_0 = p_1 = \frac{1}{2}$. According to the table in Figure 9(b), the optimum displacement is $|\beta|^2 = 0.574, |\beta| = 0.757$, yielding threshold

$$\eta = 4\sqrt{|\alpha||\beta|}/\log_e(|\beta+\alpha|^2/|\beta-\alpha|^2) = 4\sqrt{(0.447)(0.757)}/\log_e(1.45/0.096) = 2.3/2.7 = 0.86$$

The conditional correct detection probabilities are $P(C|H_0) = p(k < \eta|K_{(-)}) = \exp(-K_{(-)}) = 0.933$ for the null hypothesis and $P(C|H_1) = 1 - p(k < \eta|K_{(+)}) = 1 - \exp(-K_{(+)}) = 0.765$ for the alternate, yielding $P(C) = p_0 P(C|H_0) + p_1 P(C|H_1) = \frac{1}{2}(0.933 + 0.765) = 0.849$. The average error probability follows as $P(E) = 1 - P(C) = 0.151$. This result is shown in Figure 10 as the single point labeled "Numerical Example 1" on the "Optimized Kennedy Receiver" performance curve, which was computed numerically over the range of values $0 < |\alpha|^2 < 0.8$. Note that the optimized Kennedy receiver approach first described in [10] outperforms the Kennedy receiver for all signal energies, and in addition it even outperforms the coherent receiver at small signal energies where coherent detection approaches the Helstrom bound, as we have shown with the help of the small-energy model. However, it does not maintain this improvement over the Kennedy receiver for large symbol energies, but rather begins to approach the performance of the Kennedy receiver as the signal energy increases.

The above derivation suggests that by applying the optimum displacement to the BPSK signals prior to photon-counting detection, lower error probabilities will be obtained than possible with the Kennedy receiver, for any signal energy. The measurement-state derivation above also suggests that for the case of small signal energies, the Helstrom bound may be approached by the optimized Kennedy receiver, since the displacement of the signal states

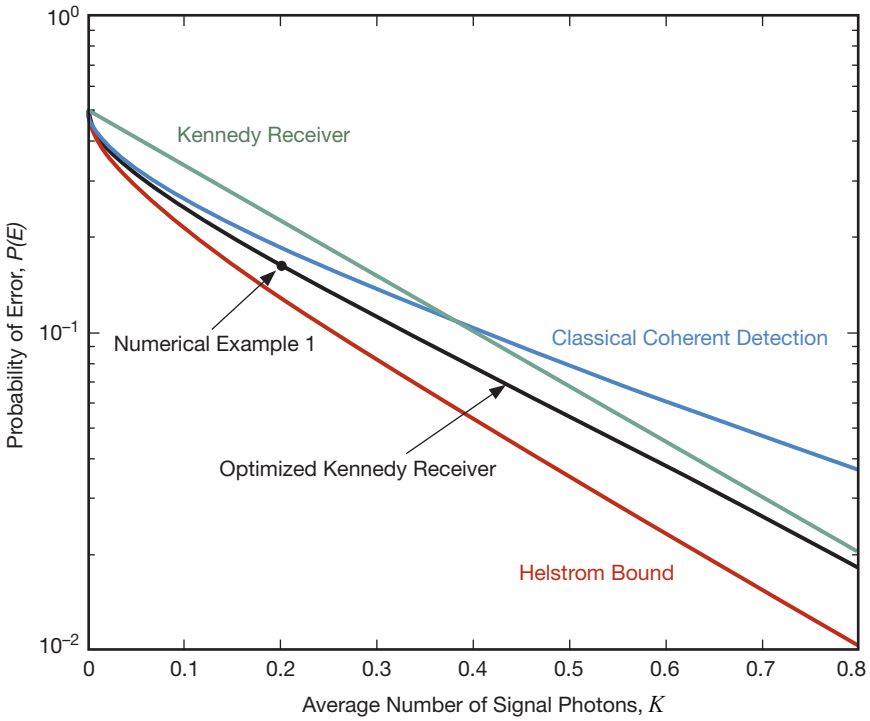

Figure 10. Error probability performance of coherent, Kennedy, and optimized Kennedy receivers.

is in the direction of the optimum measurement, where the measurement states are placed symmetrically around the signal states $|0\rangle,|1\rangle$ plane. As a heuristic check, we note that as the signal energy approaches zero the optimum displacement approaches $|\beta^*|^2 = 0.5$, or $|\beta| = 0.707$, which now projects significantly onto higher number-state dimensions (as can be seen in Figure 7, where the probability of projecting onto a higher dimension is seen to be 0.09). Hence the measurement states no longer reside entirely in the $|0\rangle,|1\rangle$ plane, and the photon-counting interpretation for displaced signal states is not strictly valid. Nevertheless, displaced photon-counting still approximates the optimum quantum measurement in this region, hence error probabilities close to the Helstrom bound can be achieved with this technique.

IV. Approaching the Quantum Limit via Partitioned Detection

As shown above, the Helstrom bound can be approached closely by classical measurement techniques such as coherent detection, provided the signal energy approaches zero. However, uncoded error probabilities obtained with small signal energies generally do not meet optical communications requirements, since even modern codes require uncoded bit-error probabilities of 0.1 or less for rate 1/2 codes. The above results show that the optimized Kennedy receiver approaches the Helstrom bound for small signal energies, but reverts back to the performance of the Kennedy receiver for higher signal energies, where modern optical communications systems operate. This suggests that the advantages of the near-optimum small-signal-energy measurement should be incorporated into the overall detection strategy, in order to extend the improved performance of the optimized Kennedy receiver into the high-signal-energy region, with practically implementable optical communications receiver processing.

A. Partitioned-Interval Detection Strategy

Consider the partitioned signal detection strategy illustrated in Figure 11, where the original BPSK symbols have been converted to on-off signaling via matched displacement, as in the Kennedy receiver. Each T-second signal interval is now partitioned into two consecutive disjoint intervals: an initial interval of duration T_1 seconds, and a second interval of duration T_2 seconds. The average photon counts in these two intervals can be denoted as $4K_1$ and $4K_2$, respectively, with corresponding photon counts of k_1 and k_2. As indicated, the first interval is intended to be short, providing a small-energy (hence high-quality) "predetection" measurement, whereas the second interval is intended to supply more signal energy to further lower the error probability to acceptable levels for communication.

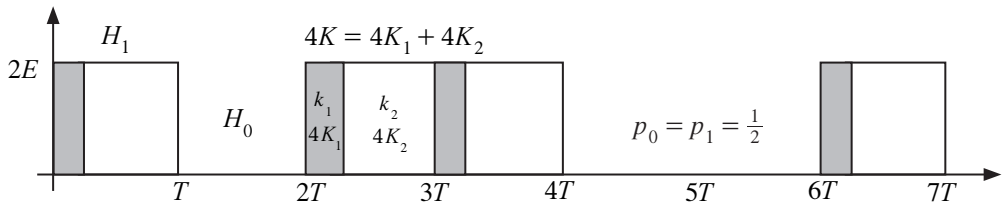

Figure 11. Signal model for the partitioned interval detection strategy.

Based on the observation that for the Kennedy receiver, correct detection occurs whenever the cancelled signal (null hypothesis) is observed, the strategy is to try to "guess" the correct hypothesis with a near-optimum measurement in the first interval, and cancel the signal in the second interval by applying the appropriate displacement whenever a signal is predetected. If no signal is detected in the first interval, then the receiver continues to count photons in the second interval, without cancellation. This is similar to the approach used by the Dolinar receiver, which, however, must respond instantaneously to each photon-detection event wherever it may occur within the signal interval, whereas here the counting intervals are defined based on predictable average signal energies instead of unpredictable photon occurrence times. Since with equal a priori probabilities roughly half of the original signal intervals contain no signal energy, it follows that any correct detection in the predetection interval will lead to more cancelled signals being observed in the second interval than in the original sequence. The final decision is based on the presence or absence of photon counts observed in the second interval, but also takes into account the outcome of the predetection, which controls the application of the cancelling displacement.

This two-step detection strategy can be summarized in the following algorithm:

If $k_1 > 0$, add 180 deg to the local field, continue counting:	if $k_2 = 0$, decide H_1
If $k_1 = 0$, continue counting:	if $k_2 > 0$, decide H_1
If $k_1 = 0$, continue counting:	if $k_2 = 0$, decide H_0

This detection strategy is equivalent to a "modified sequence" interpretation, where some of the pulses in the second segment have been cancelled due to correct identification of the pulse in the first segment. Restricting our attention to the second segment only, we find that this new sequence has more cancelled pulses than the original sequence where the a priori probabilities were equal. Therefore, if we observed only the modified sequence (where some

of the original pulses have now been cancelled due to correct "predetection" decisions, but no new pulses have been added), then we would assign a higher probability to the occurrence of nulls in the second interval. Based on observing the modified sequence, we would conclude that the a priori probabilities p_0', p_1' of this new sequence were in fact not equal, but rather given by the expressions $p_0' = p_0 P(C|H_0) + p_1 P(C|H_1)$ and $p_1' = 1 - p_0'$. Representations of the modified sequence are shown in Figure 12(a) and 12(b), where the intermediate decisions are shown in (a) and the final sequence in (b): for example, the second segment in the third symbol-interval ($2T < t \le 3T$) has been cancelled due to a correct decision in the first segment of this same interval, because a count $k_1 > 0$ has been observed in the first interval.

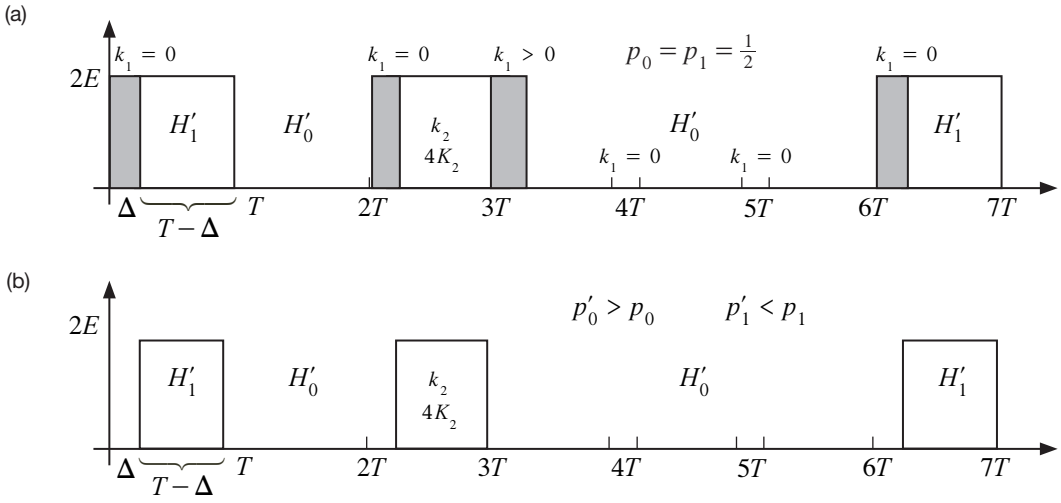

Figure 12. (a) Original and (b) modified sequences, after a single correct predetection measurement.

The modified sequence appears to have more null-hypotheses H_0' and fewer alternatives H_1'. The decision strategy for the modified sequence shown in Figure 12(b), in terms of the modified a priori probabilities $p_0' > p_0$ and $p_1' < p_1$, can be re-stated as follows:

$$\begin{aligned} &\text{If } k_2 > 0, && \text{declare } H_1' \\ &\text{If } k_2 = 0, && \text{declare } H_0' \end{aligned}$$

However, now we must keep track of the correct decisions in the predetection segment that lead to pulse-cancellations, in order to detect the original message.

We can write the probability of correct detection and the probability of error for the modified sequence in terms of the modified a priori probabilities, as

$$\begin{aligned} P(C) &= p_0' P(C|H_0') + p_1' P(C|H_1') = (1 - p_1') P(C|H_0') + p_1' P(C|H_1') \\ &= P(C|H_0') - p_1' [P(C|H_0') - P(C|H_1')] \\ P(E) &= 1 - P(C) = 1 - P(C|H_0') + p_1' [P(C|H_0') - P(C|H_1')] \end{aligned} \tag{6}$$

Note that $P(C|H_0') \neq 1$ in general. Recalling that p_1' represents the probability of making an error in the first segment, and that the modified hypotheses $H_i', i = 0,1$ refer to the second segment, we can see that the final error probability can always be improved by reducing p_1', provided that $P(C|H_0') > P(C|H_1')$, which is satisfied by the detection processes considered here, namely, the Kennedy and optimized Kennedy receivers in the region of interest. Therefore, we can potentially chose a detection technique in the first segment that closely approaches the Helstrom bound for small signal energies, and perhaps a different detection strategy in the second segment, in order to achieve the desired error probability for communications applications. This result forms the basis of the "partitioned" approach, which we now examine for several cases of interest.

For the case of signal cancellation followed by photon-counting detection, the relevant probabilities for the modified sequence become

$$H_0': \;\; p(k_2 = 0) = 1, \;\; H_1': \;\; \begin{cases} p(k_2 = 0) = \exp(-4K_2) \\ p(k_2 > 0) = 1 - \exp(-4K_2) \end{cases}$$

which yield the following conditional probabilities of correct detection: $P(C|H_0') = 1$, and for the alternate hypothesis, $P(C|H_1') = 1 - \exp(-4K_2)$. Substituting into Equation (5) yields

$$P(C) = p_0' + p_1'[1 - \exp(-4K_2)] = 1 - p_1' \exp(-4K), P(E) = 1 - P(C) = p_1' \exp(-4K_2)$$

Note that if $p_1' = \frac{1}{2}\exp(-4K_1)$, as would be obtained with photon-counting detection over the first segment, then the error probability after observing the entire symbol interval would simply become $\frac{1}{2}\exp(-4K)$, which is exactly the same as for the Kennedy receiver, hence nothing would be gained. However, it also suggests that if $p_1' < \frac{1}{2}\exp(-4K_1)$, the error probability of the modified sequence will decrease correspondingly, resulting in $P(E) < \frac{1}{2}\exp(-4K)$. This approach provides a means for approaching the Helstrom bound by employing a better detection strategy in the first segment than simple field cancellation followed by photon-counting, resulting in better overall performance. With $P_K(E), P_c(E)$ and $P_{0K}(E)$ referring to the Kennedy, coherent, and optimized Kennedy receivers, respectively, the best strategy can be inferred from the ratio of the error probabilities $P_K(E)/P_c(E)$ and $P_K(E)/P_{0K}(E)$ in Figure 13, which is interpreted as "gain over the Kennedy receiver." Note that in Figure 13, N refers to the total number of segments used by the partitioned receiver, as explained subsequently in Section IV.B, "Optimized N-Segment Receiver."

In Figure 13, the coherent receiver peaks at $K_s = 0.095$, attaining a maximum gain of 1.272 over the Kennedy receiver, whereas the optimized Kennedy receiver peaks at $K_s = 0.165$, with a maximum gain of 1.381, after which both gains decrease: the optimized Kennedy receiver approaches 1 at high signal energies, reverting back to the conventional Kennedy receiver, whereas the gain of the coherent receiver continues towards zero.

The following example illustrates the calculation of the error probability for the two-segment partitioned receiver at the point $K_s = 0.5$, with the optimum partition having been determined numerically by varying T_1 and applying the optimum displacement to each segment. For this example, the optimum partition turned out to be $K_{s,1} = 0.04$, $K_{s,2} = 0.46$,

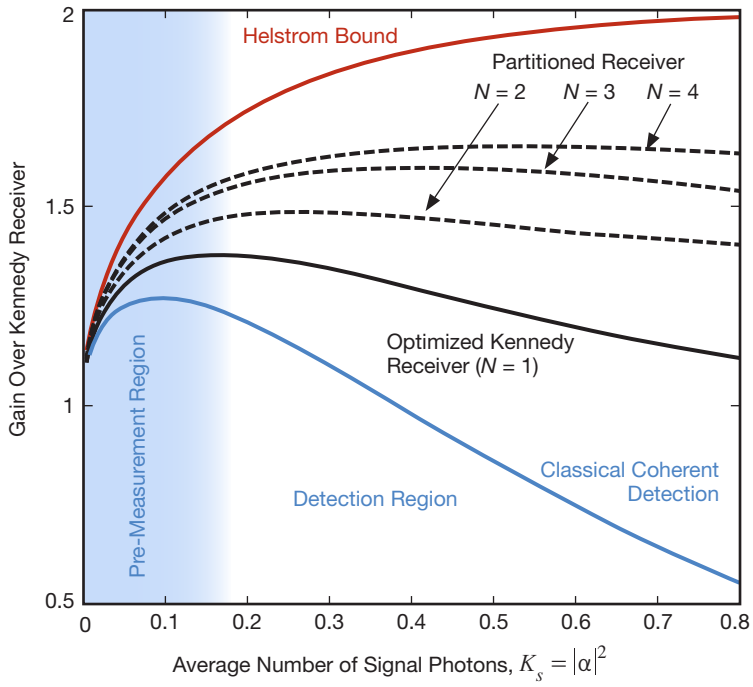

Figure 13. Gain of coherent, optimized Kennedy, and partitioned receivers over Kennedy receiver.

for total signal energy of $K_s = 0.5$. Note that, as expected, much less signal energy is used in the first segment than in the second.

Example 2. We now let $K_s = |\alpha|^2 = 0.5$ for the total signal energy, and find the optimum displacement by solving the transcendental equation for the equi-probable case (as shown in Figure 9), yielding $\beta_1^* = 0.7168$ and $\alpha_1 = 0.6782$. It can be inferred from Figure 3 that the optimum threshold is zero in this region. In the first segment we have $K_{1,(-)} = |\beta_1^* - \alpha_1|^2 = 0.2671$ under the null hypothesis and $K_{1,(+)} = |\beta_1^* + \alpha_1|^2 = 0.841$ for the alternate, which yield the conditional probabilities $P(C|H_0) = p(k_1 = 0|K_{1,(-)}) = \exp(-K_{1,(-)}) = 0.766$ for the null hypothesis, and $P(C|H_1) = 1 - p(k_1 = 0|K_{1,(+)}) = 1 - \exp(-K_{1,(+)}) = 0.568$ for the alternate.

The probability of correct detection becomes

$$P(C) = p_0 P(C|H_0) + p_1 P(C|H_1) = \tfrac{1}{2}(0.766 + 0.568) = 0.667 \equiv p_0'$$

and the error probability follows as $P(E) = 1 - P(C) = 0.333 \equiv p_1'$. As explained above, these detection probabilities are viewed as a priori probabilities for the new sequence, since whenever a correct predetection occurs (with probability p_0'), the field in the second segment is effectively cancelled, otherwise it remains unchanged (with probability p_1'). We have therefore created a new sequence consisting only of the second segment of each symbol, where the nulls designated by H_0' outnumber the original nulls, and the pulses (designated by H_1') are now fewer, since some pulses have been predetected correctly and subsequently cancelled in the second segment.

If we decided to apply cancellation with photon-counting in the second segment, which corresponds to the conventional Kennedy receiver but with partitioning correspond-

ing to the optimized Kennedy receiver, then under H_0' correct detection would always follow, $P(C|H_0') = 1$, while under H_1' correct detection would occur with probability $P(C|H_1') = 1 - \exp(-4K_2) = 0.841$. The average error probability for this approach becomes $P(E) = 1 - p_0' P(C|H_0') - p_1' P(C|H_1') = 0.053$. This result is shown in Figure 14, at $K_s = 0.5$: note that it is significantly lower than that of the Kennedy receiver, even slightly lower than the optimized Kennedy receiver, but not nearly as good as the optimized two-segment receiver.

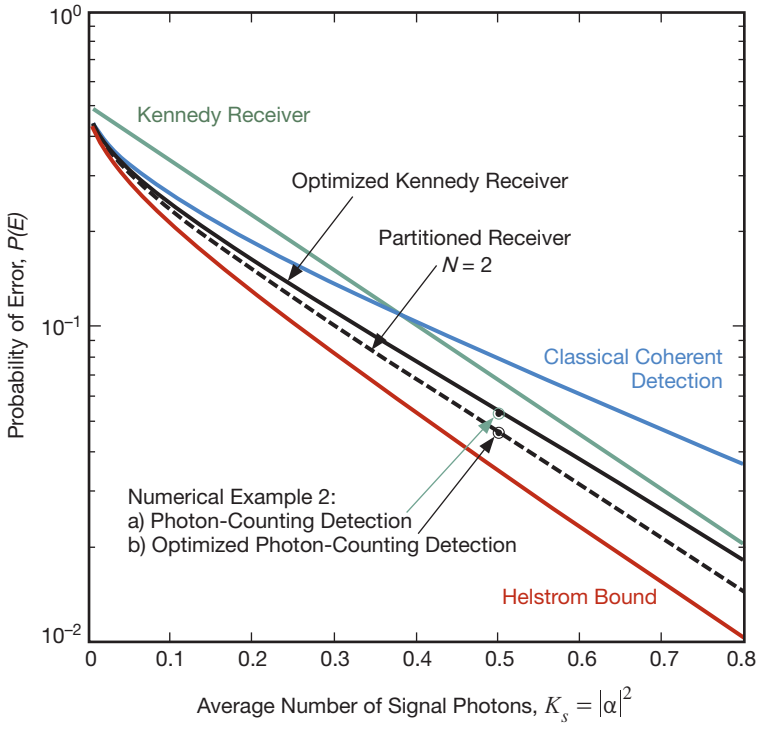

Figure 14. Error probability performance and comparison of two-segment partitioned receiver.

In order to confirm the performance of the optimized two-segment receiver, we need to add the optimum local field to the received field in the second segment, which must now be computed for the new a priori probabilities $p_0' = 0.667$ and $p_1' = 0.333$. For these conditions, we obtained $\beta_2^* = 0.7682$, $\alpha_2 = 0.6782$, $K_{2,(-)} = |\beta_2^* - \alpha_2|^2 = 0.0081$, $K_{2,(+)} = |\beta_2^* + \alpha_2|^2 = 2.092$, yielding the conditional probabilities $P(C|H_0') = p(k_2 = 0|K_{2,(-)}) = \exp(-K_{2,(-)}) = 0.992$ and similarly $P(C|H_1') = 1 - p(k_2 = 0|K_{2,(+)}) = 1 - \exp(-K_{2,(+)}) = 0.877$. The average error probability of the optimized two-stage receiver is $P(E) = 1 - p_0' P(C|H_0') - p_1' P(C|H_1') = 0.046$, which coincides with the numerically derived curve as shown in Figure 14. This example helps to verify the accuracy of the numerical program that generated the results in Figure 14.

B. Optimized *N*-Segment Receiver

The optimized two-segment detection approach described above can be extended directly to three or more segments, by considering the first *N*–1 segments of an *N*-segment receiver to be a "predetection" segment whose decision outcome modifies the a priori probabilities of the final modified sequence, improving the fidelity of the final decision. For example, the

performance of a three-segment receiver can be evaluated by starting out as a two-segment receiver, but then partitioning the relatively small predetection interval into two segments and optimizing each before optimizing the error probability for the third segment, further improving receiver performance. This procedure extends directly to an arbitrary number of segments, each step yielding an improvement over the previous step, but also increasing the complexity of the receiver.

The gain over the Kennedy receiver for up to four optimized segments reaches a maximum at slightly higher signal energies, as can be seen in Figure 13, which flatten out as the number of segments increases, effectively maintaining the maximum gain achieved by the predetection measurement over the region of interest. For three- and four-segment optimized receivers, the maxima occur at $K_s = 0.38$ and $K_s = 0.62$ average signal photons. The gain curves can be divided roughly into two regions — a "predetection" region over which the gains rise rapidly, followed by a "detection" region over which the gains flatten out attempting to maintain maximum gain. The boundary between these two regions is roughly the initial small-energy region up to approximately 0.2 signal photons as shown in Figure 13. This interpretation is in line with our previous conclusion that displacement followed by photon-counting is close to the optimum strategy at small signal energies; hence, we can interpret any measurement made within this region in a segmented receiver approach to be a predetection measurement: the use of multiple segments is merely a means to obtain better predetection performance. It should be noted that any other predetection strategy that improves upon these initial error probabilities will lead to comparable gains in overall performance. Therefore, other measurement techniques that may be developed in the future could also be used to carry out predetection, potentially leading to further improvements in overall receiver performance.

The error probability performance of optimized two, three and four segment receivers are shown in Figure 15 along with that of the Kennedy receiver, coherent receiver and optimized Kennedy receiver for comparison. The partitioned receiver discussed here outperforms the previously known "near-optimum" approaches such as the Kennedy receiver for all signal energies, with gains of more than 2 dB over the Kennedy receiver at $P(E) = 0.1$, in the region of greatest interest for coded optical communications. This new approach effectively partitions the signal interval into two segments — a predetection segment that employs displaced photon-counting to closely approach the Helstrom bound at small signal energies, followed by a detection segment that measures the remaining signal energy to achieve the desired communications performance.

For any number of predetermined segments N, the result of the first $(N–1)$ decisions is incorporated into the probability of correct detection p_0' based on the first $(N–1)$ segments, which is used as the a priori probability of hypothesis H_0' for the final segment. This strategy can be implemented using a bank of N lasers and switching between them using offset clocks operating at the symbol rate, hence leads to practically implementable receivers for small values of N, but it also highlights the reason for suboptimal performance when compared to the Dolinar receiver: since photons arrive randomly within any predetermined decision interval, the signal energy after a photon detection event is effectively wasted with the partitioned-interval approach since the decision could actually be made as soon as a photon is

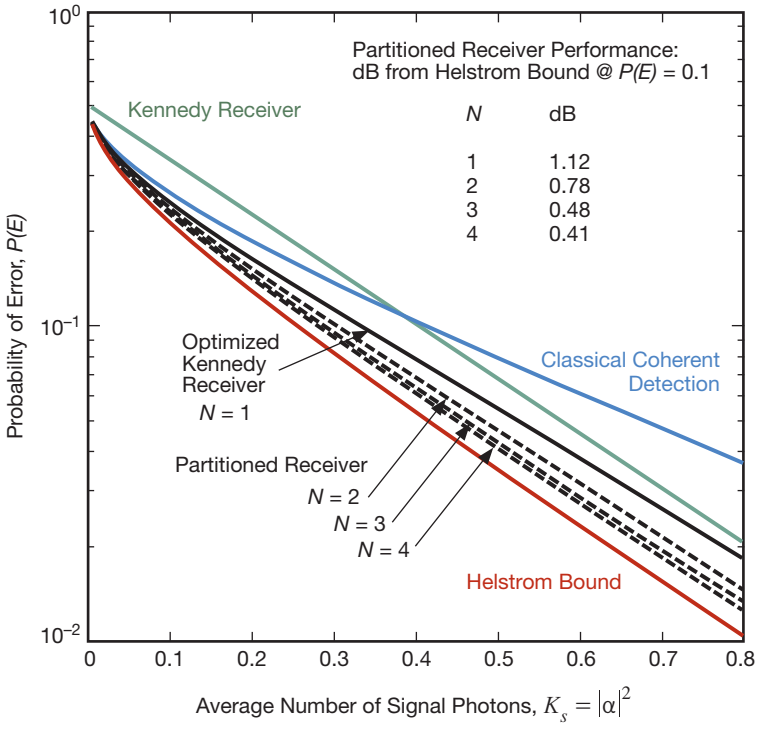

Figure 15. Error probability performance and comparison of *N*-segment partitioned receivers.

detected. However, that requires processing bandwidth far exceeding the signal bandwidth, and hence leads to problems with implementation, particularly at high data rates. This is one of the fundamental differences between the two approaches, which is minimized as the number of segments increases: the Dolinar receiver requires infinite processing bandwidth to reach the Helstrom bound together with precisely controlled continuous-time laser intensities, whereas the partitioned-interval approach switches between a few local lasers with predetermined intensities at the signaling rate, but does not reach the Helstrom bound for small, hence practical, values of *N*.

C. Practical Implementation of the Partitioned-Interval Receiver

In the context of practical optical communications, the receiver must establish phase lock between the received and local laser fields, combine these fields optimally to effect displacement using a beam-splitter, and establish synchronization on the symbol level in order to carry out the detection operation. Symbol synchronization is equivalent to running a clock at the same rate as the received data stream, to identify the symbol boundaries required for photon-counting detection. With a two-segment receiver, the displacement of the signal in each interval is different, due to both different signal energies and a priori probabilities, which implies that two or more local lasers set to different intensities could be toggled or a single laser could be switched rapidly between two preset values, in a high-data-rate scenario. Note that the required laser intensities and optimum partitions can be precomputed based on knowledge of the received signal energy (which is typically slowly varying in deep-space applications), hence real-time optical feedback is not required with this approach.

V. Summary and Conclusions

A novel optical communications receiver concept capable of approaching the quantum limit in the region of interest for coded optical communications from deep space has been developed and analyzed in this article. The key idea is to break up the signal interval into a short "predetection" segment followed by a longer validation segment in such a way as to optimize overall performance. This two-interval interpretation was extended to higher complexity N-interval detection by interpreting the processing in the first N–1 intervals as an improved predetection measurement, viewing the final N^{th} interval as the validation segment. It is shown that increasing N leads to improved performance for N = 2, 3, and 4 segments, arguably approaching the quantum limit for larger N but only at the cost of greater processing complexity. Therefore, this approach is intended primarily for low-complexity applications where improved receiver performance is deemed necessary. It was shown that with four disjoint segments, performance of the partitioned receiver approached the Helstrom bound to within 0.41 dB, or equivalently improved upon the Kennedy receiver by 2 dB, at an error probability of 0.1 typically required by modern codes. A laboratory demonstration of this segmented detection approach would help to clarify the technological challenges that must be solved in order to enable high-data-rate optical communications near the quantum limit for future deep-space missions.

References

[1] C. W. Helstrom, *Quantum Detection and Estimation Theory*, Mathematics in Science and Engineering, New York: Academic Press, 1976.

[2] C.-W. Lau, V. A. Vilnrotter, S. Dolinar, J. M. Geremia, and H. Mabuchi, "Binary Quantum Receiver Concept Demonstration," *The Interplanetary Network Progress Report*, vol. 42-165, Jet Propulsion Laboratory, Pasadena, California, pp. 1–8, May 15, 2006. http://ipnpr.jpl.nasa.gov/progress_report/42-165/165H.pdf

[3] R. Cook, P. Martin, and J. M. Geremia, "Optical Coherent State Discrimination Using a Closed-Loop Quantum Measurement," *Nature*, vol. 446, no. 7137, pp. 774–777, April 12, 2007.

[4] M. Sasaki and O. Hirota, "Optimum Decision Scheme with a Unitary Control Process for Binary Quantum-State Signals," *Physical Review A*, vol. 54, no. 4, pp. 2728–2736, October 1996.

[5] A. Acin, E. Bagan, M. Baig, L. Masanes, and R. Munoz-Tapia, "Multiple-Copy State Discrimination with Individual Measurements," *Physical Review A*, vol. 71, no. 3, pp. 032338-1–032338-5, March 23, 2005.

[6] R. J. Glauber, "Coherent and Incoherent States of the Radiation Field," *Physical Review*, vol. 131, no. 6, pp. 2766–2788, September 15, 1963.

[7] V. A. Vilnrotter and C-W. Lau, "Quantum Detection and Channel Capacity for Communications Applications," *Proceedings of SPIE*, vol. 4635, pp. 103–115, 2002.

[8] S. M. Barnett and P. M. Radmore, *Methods in Theoretical Quantum Optics*, Oxford Series in Optical and Imaging Sciences, Oxford: Clarendon Press, 1997.

[9] M. Paris, "Displacement Operator by Beam Splitter," *Physics Letters A*, vol. 217, nos. 2–3, Elsevier, pp. 78–80, July 8, 1996.

[10] A. Assalini, N. D. Pozza, and G. Pierobon, "Revisiting the Dolinar Receiver through Multiple-Copy State Discrimination Theory," arXiv: 1107.5452v2, August 3, 2011.

[11] C. Wittmann, M. Takeoka, K. Cassemiro, M. Sasaki, G. Leuchs, and U. Andersen, "Demonstration of Near-Optimal Discrimination of Optical Coherent States," *Physical Review Letters*, vol. 101, no. 21, pp. 210501-1–210501-4, November 21, 2008.